Supporting Information

Araya et al. 10.1073/pnas.1321869111

SI Text

Correlations Between Morphological and Physiological Spine Parameters. We further explored the database of 12 spines with minimal stimulation synaptic responses and used it to search for additional correlations between the morphological characteristics of spines and their functional parameters of their excitatory postsynaptic potentials (EPSPs; Fig. S2). We first analyzed the effect of the location of the spine along the dendritic tree, because dendritic cable properties affect EPSP kinetics and amplitude (1). Nevertheless, in our database, which only included spines relatively close (<100 μm) to the soma, we did not detect any systematic correlation between any functional or morphological parameter of the spines and its somatic distance. Specifically, there were no significant correlations between the distance from the spine to the soma and EPSP amplitude (r^2 = 0.01, P = 0.75), amplitude of calcium response (ΔF/F, r^2 = 0.007, P = 0.79), or spine head diameter (r^2 = 0.036, P = 0.55). Importantly, there was no correlation between spine neck length and distance from the soma (r^2 = 0.005, P = 0.83; Fig. S2), in agreement with previous two-photon and electron microscopy reconstructions of these neurons (2, 3), which ruled out somatic proximity as a factor for why longer spines in our data set generated smaller somatic voltage responses.

We also wondered if the inverse correlation between EPSP and neck length could be explained by a correlation between spine head and EPSP amplitude (4). As previously reported for uncaging evoked potentials (2), we did not find a correlation between EPSP amplitude and spine head diameter (r^2 = 0.04, P = 0.53). Interestingly, when we restricted our analysis to spines with similar neck lengths (0.2 μm in length, which represent our largest sample of spines), we found a significant correlation between spine head diameter and uncaging potential (r = 0.87, P < 0.001, n = 11 spines), indicating that the EPSP amplitude is indeed correlated with the spine head diameter, once the spine neck length effect on EPSP amplitude is accounted for. In addition, we found no relation between spine head diameter and neck length in our measurements (r^2 = 0.001, P = 0.96), consistent with previous optical or ultrastructural studies in these neurons (2, 3, 5), indicating that the morphologies of the spine head and neck are regulated independently.

We also examined the correlation between the 10–90% rate of rise of the EPSPs with the neck length, we found a significant negative correlation [r^2 = 0.43, P < 0.05 (P = 0.0195)], similar to that found with uncaging potentials (2), and also a strong correlation between the 10–90% rate of rise and the amplitude of the EPSPs (r^2 = 0.74, P < 0.01; Fig. S2, red lines). There was no correlation between the 10–90% rate of rise of the EPSPs with somatic proximity (r^2 = 0.01, P = 0.72), spine head diameter (r^2 = 0.19, P = 0.15), or peak calcium accumulations (ΔF/F, r^2 = 0.029, P = 0.59). Finally, there was no relation between the distance to the stimulation electrode and the spine head diameter (r^2 = 0.216, P = 0.128), spine neck length (r^2 = 0.014, P = 0.716), somatic proximity of the spine (r^2 = 0.377, P = 0.034), or with the 10–90% rate of rise of the EPSP (r^2 = 0.031, P = 0.585), EPSP amplitude (r^2 = 0.039, P = 0.539), or peak calcium response (ΔF/F, r^2 = 0.073, P = 0.396).

1. Rall W, Segev I, Rinzel J, Shepherd GM (1995) *The Theoretical Foundation of Dendritic Function: Selected Papers of Wilfrid Rall with Commentaries* (MIT Press, Cambridge, MA).
2. Araya R, Jiang J, Eisenthal KB, Yuste R (2006) The spine neck filters membrane potentials. *Proc Natl Acad Sci USA* 103(47):17961–17966.
3. Arellano JI, Benavides-Piccione R, DeFelipe J, Yuste R (2007) Ultrastructure of dendritic spines: Correlation between synaptic and spine morphologies. *Front Neurosci* 1(1): 131–143.
4. Matsuzaki M, et al. (2001) Dendritic spine geometry is critical for AMPA receptor expression in hippocampal CA1 pyramidal neurons. *Nat Neurosci* 4(11):1086–1092.
5. Benavides-Piccione R, Ballesteros-Yáñez I, DeFelipe J, Yuste R (2002) Cortical area and species differences in dendritic spine morphology. *J Neurocytol* 31(3-5):337–346.
6. Arellano JI, Espinosa A, Fairén A, Yuste R, DeFelipe J (2007) Non-synaptic dendritic spines in neocortex. *Neuroscience* 145(2):464–469.

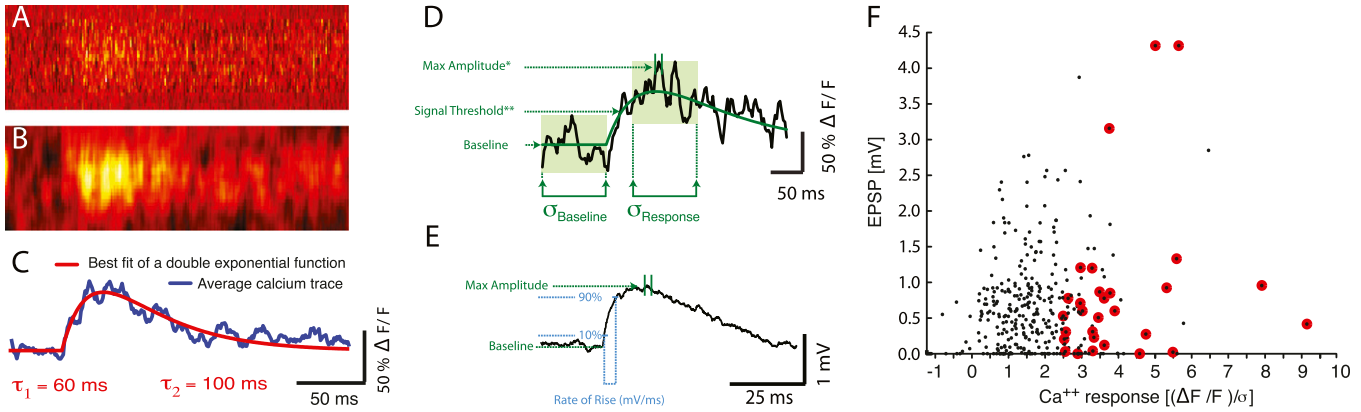

Fig. S1. Automatic detection of minimal stimulation events. Method of analysis: Creating a double exponential function kernel to fit Ca^{2+} responses: (*A*) Average raw response of five handpicked calcium traces with clear calcium responses. (*B*) Gaussian low-pass filtered average response from *A*. (*C*) Spatial average of all line scans (blue trace) and the best fit of a double-exponential (red trace) with tau1 (t1) = 60 ms and tau2 (t2) = 100 ms. (*D*) Calcium traces were identified as positive if all three of the following conditions were met: (*i*) The average amplitude of a 5-ms window centered on the maximum of the signal (labeled with an asterisk) within the first 50 ms after the stimulus was at least 2.5× greater than the SD of 50 ms of the baseline signal before the stimulus (this threshold is labeled with double asterisks, **); (*ii*) The populations of data points from −50 to 0 ms (labeled σbaseline) and from +10 to +60 ms (σResponse) (where 0 ms marks the occurrence of the stimulus) were significantly different as determined by a Student's *t* test; and (*iii*) The shape of the first 100 ms of the signal after stimulus could be fit to a double exponential with previously determined time constants (green line). (*E*) Voltage traces were analyzed (after deletion of a stimulus artifact) for their maximum amplitude, measured as the difference of the average of two 5-ms time windows, one centered on −3 ms before stimulus and the other on the maximum voltage deflection within 50 ms after the stimulus occurred. The rate of rise of nonzero EPSPs was measured as the difference between the voltage responses when the membrane potential reached 10% and 90% of the maximum voltage deflection divided by the 10–90 rise time (tV90%−tV10%). (*F*) Summary plot of all measured Ca^{2+} and voltage response pairs in units of the SD of the baseline ΔF/F and mV, respectively. Data points in red mark the positively identified Ca^{2+} responses as described above.

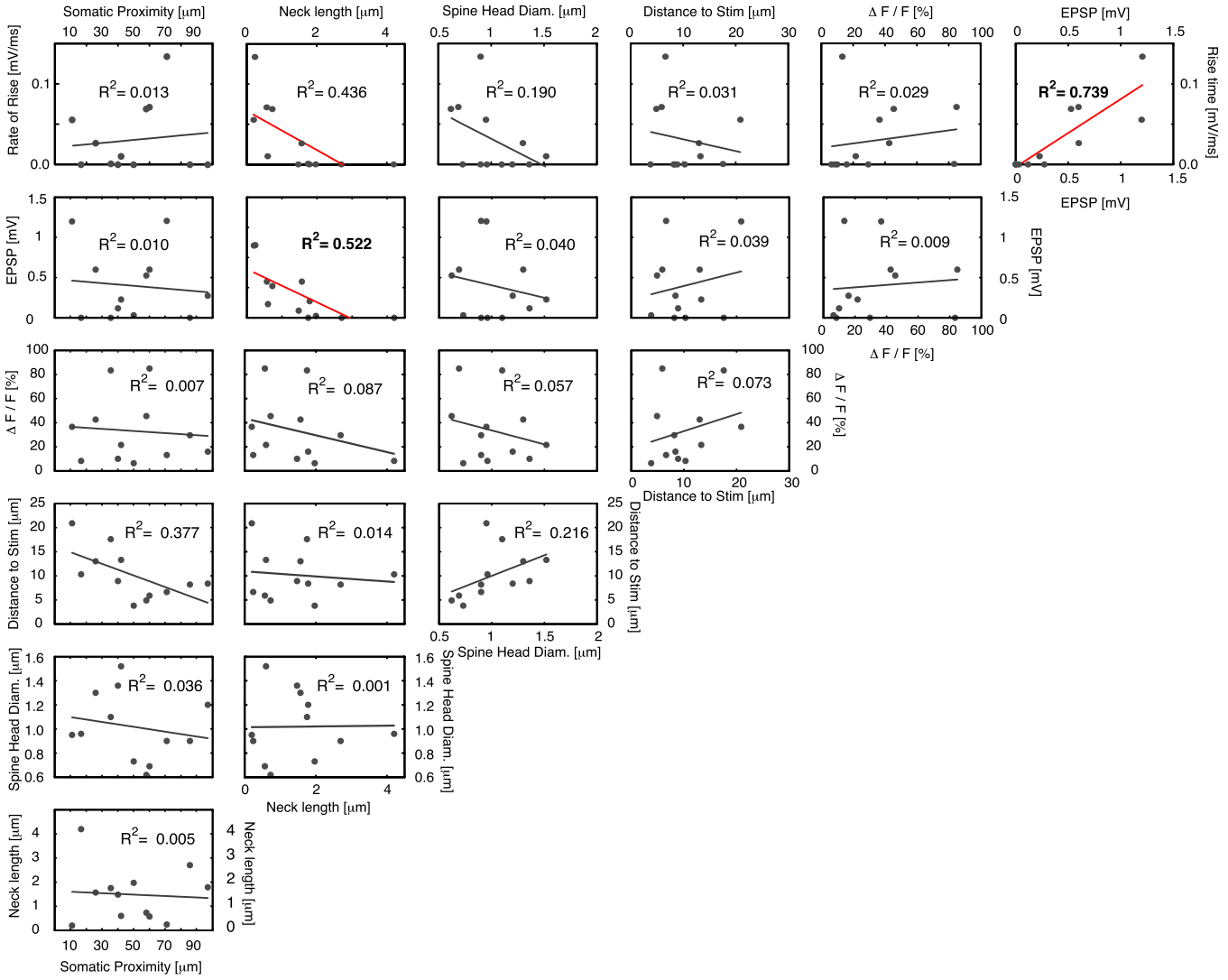

Fig. S2. Correlational analysis of morphological and electrical variables. Correlations between various experimental and morphological features such as EPSP amplitude and rate of rise, Ca^{2+} response amplitude, spine neck length, spine head diameter, somatic proximity of the stimulated spine, and proximity of the stimulating electrode to the spine. Most correlations are weak, as signified by low R^2 values for the best linear fit by regression. Only three fits of linear regression (bold red lines) reach $P < 0.05$ (slopes that are significantly different from zero; for values, see *Results*).

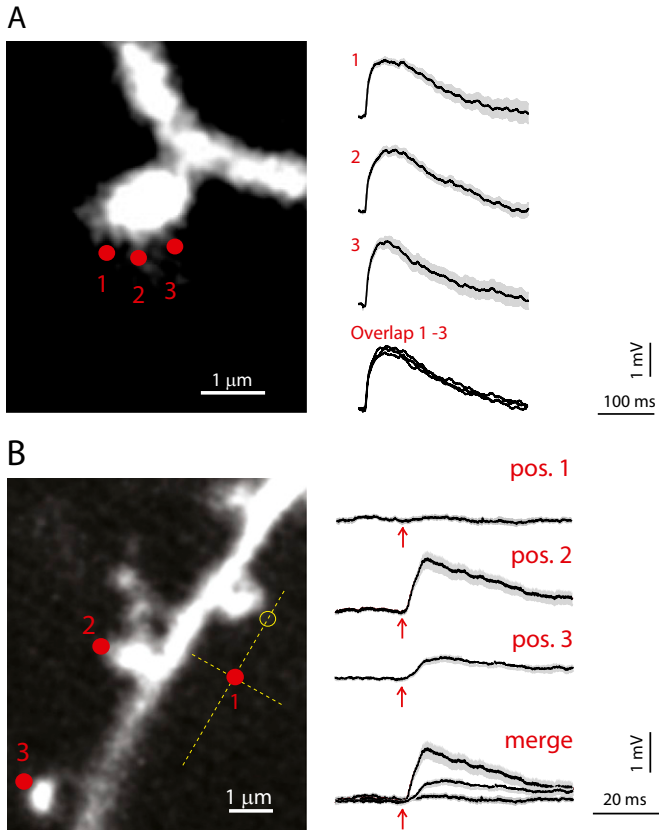

Fig. S3. Optical activation of dendritic spines, with single-spine resolution. (*A*) A layer-5 pyramidal neuron was loaded with Alexa 488 to detect and activate dendritic spines from basal dendrites. (*Left*) Higher-resolution image of a dendritic spine selected for uncaging. Red dots indicate the sites of uncaging (position 1–3). (*Right*) Traces corresponded to averages of 15 uncaging potentials recorded at the soma at the uncaging locations shown in *Left*. Note that when the voltage responses were merged, no significant differences were observed between uncaging locations (bottom traces). Shaded areas illustrate ± SEM. (*B*) A layer-5 pyramidal neuron was loaded with Alexa 488 to detect and activate dendritic spines from basal dendrites by means of two-photon uncaging of 4-methoxy-7-nitroindolinyl (MNI)-glutamate. (*B*) Spatial resolution of two-photon uncaging of MNI-glutamate. (*Left*) Red dots indicate the site of uncaging when the laser beam was parked right next to a spine (position 2 or 3) or at a location of ~1 µm away from the shaft (location 1). Note that the position 1 is at the same distance from the shaft than location 2 or the open yellow circle. (*Right*) Uncaging potentials recorded at the soma after two-photon uncaging at position 1 (pos. 1), 2 (pos. 2), or 3 (pos. 3). Note that when the laser beam was parked ~1 µm away from the shaft there was no voltage deflection generated, thus indicating that there is not glutamate spillover that activate the shaft and thus add up to the voltage deflections recorded after uncaging in short-necked spines (e.g., pos. 2). Shaded areas illustrate ± SEM.

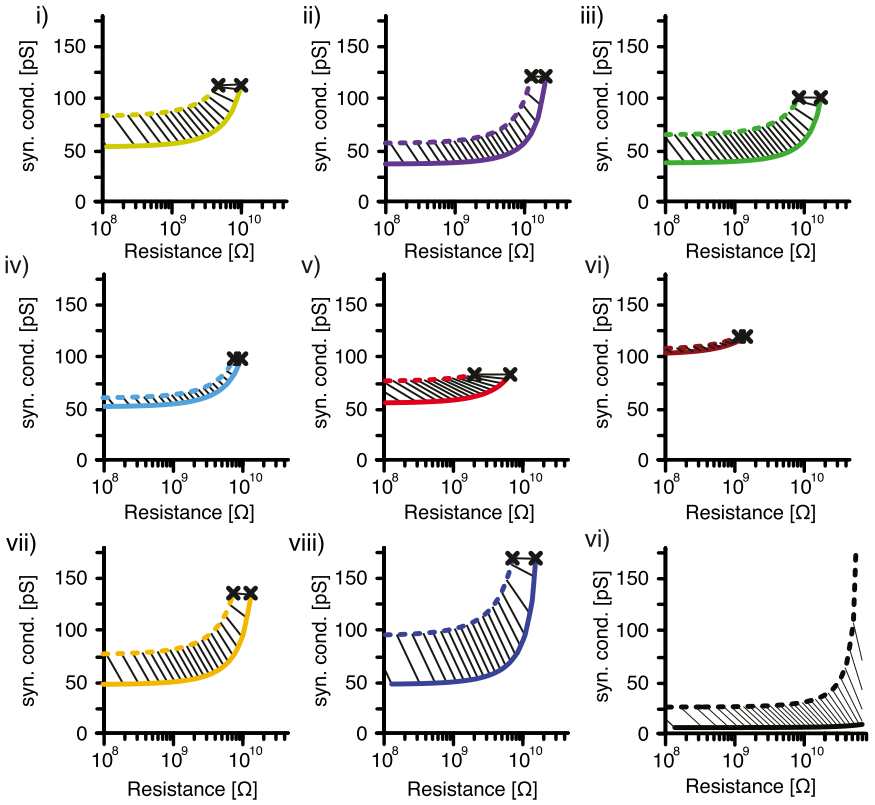

Fig. S4. Biophysical modeling of spine neck resistance and synapse conductance. Direct translation of the resistivity (ρ) values (in units of Ωcm) used in Fig. 5 into their corresponding resistances (R) (in units of Ω) for short- and long-necked spines (dotted and solid lines, respectively). The black lines connect the R values in long- (pre-STDP) and short- (post STDP) necked spines obtained from identical ρ values. A horizontal black line connecting the long- and short-necked spine signifies no conductance g change, and thus marks a single solution of conductance g and resistivity ρ values that produces the experimentally observed EPSP amplitude change (marked by black crosses).

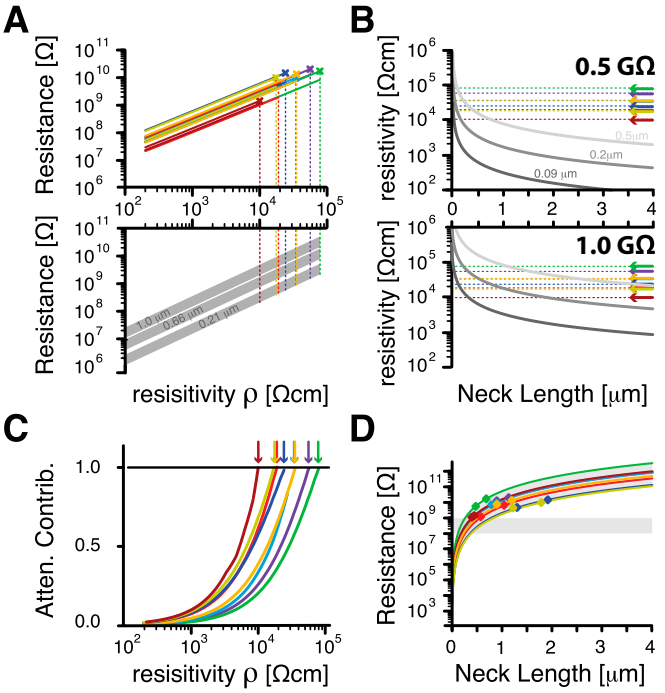

Fig. S5. Biophysical simulations of the effect of spine neck plasticity. (*A, Upper*) Resistance (*R*) values for (color-coded) long- and short-necked spines tested in Fig. 5. Crosses mark the resistance values that allowed for sole electrotonic attenuation accounting for the observed EPSP changes. (*Lower*) *R* predictions based on spine neck length normalized modeling results for various neck length [1 μm, and 0.66 and 0.21 μm (average of spine necks and minimum neck value measured by Arellano et al. (3)]. (*B*) Resistivity ρ and neck length combinations that lead to identical *R* values of 0.5 GΩ and 1 GΩ (*Upper* and *Lower*, respectively) for a given neck diameter of 0.5, 0.2, and 0.09 μm (light gray, dark gray, and black lines, respectively). Neck diameters are the maximum, average, and minimum reported diameters in a recent EM study (6). Dotted horizontal lines mark the color-coded electronic resistivity values as in previous panels. (*C*) Voltage attenuation contribution caused by the shortening of the spine neck for all resistivity values explored in Fig. 5 (without increasing *g*; *Materials and Methods*). (*D*) Prediction of resistance values based on the maximal (electrotonic-only) resistivity ρ values of the model for different neck lengths. Shaded area denotes the neck resistance regime between 0.1 and 1 GΩ.

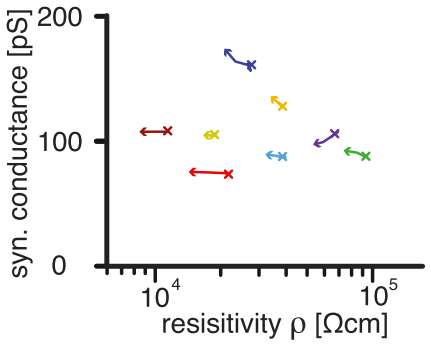

Fig. S6. Changes in spine head leak conductance. Similar to Fig. 5*D*. Conductance (*g*) and resistivity (ρ) value pairs for experiments *i–viii* (color-coded to match Fig. 5*D*) that explain the observed experimental phenomenon as a purely passive attenuation phenomenon. The lines ending in arrowheads describe the pure resistance solution with a spine head in which the membrane leak has been increased up to 100-fold.

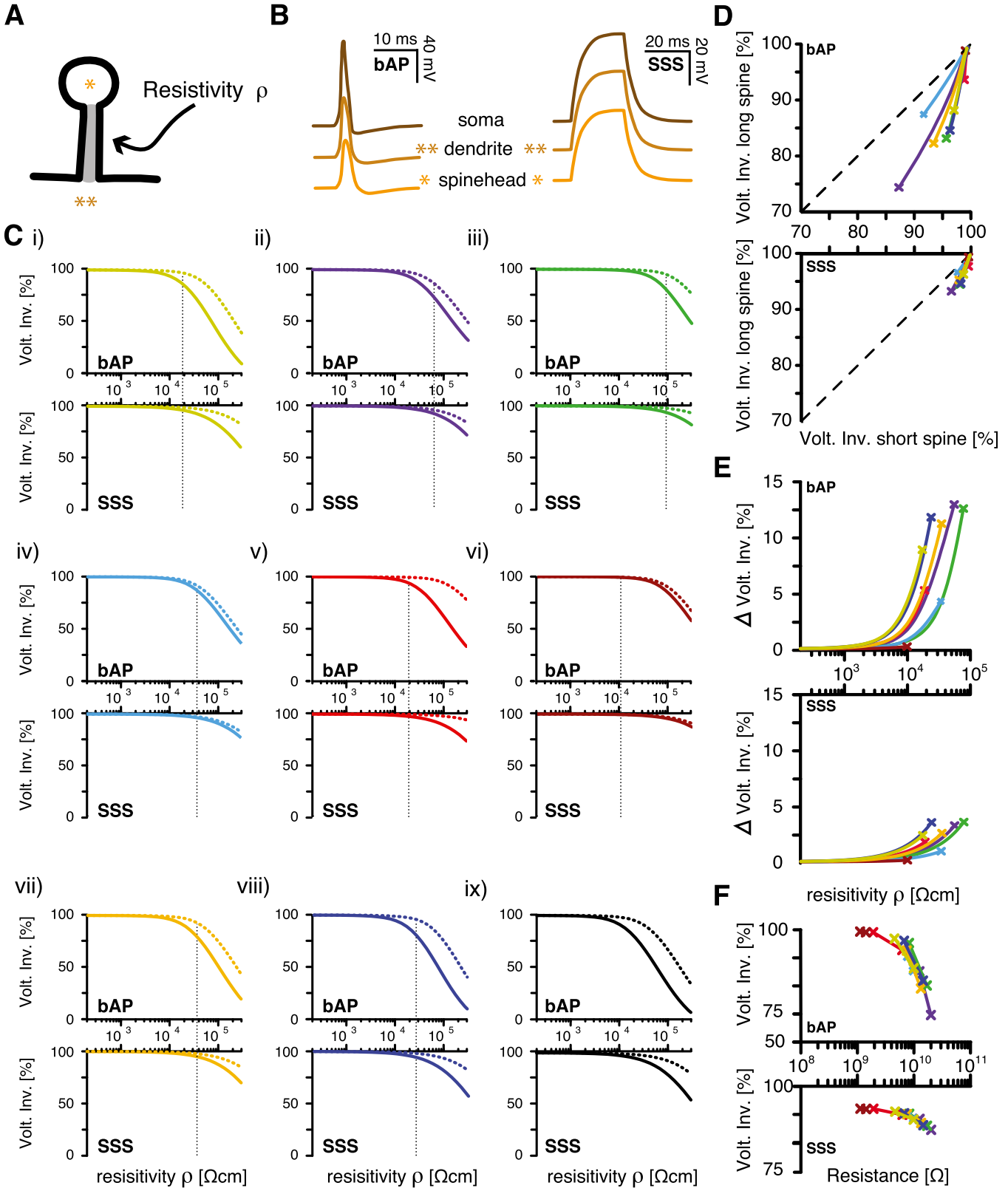

Fig. S7. Biophysical simulations to explore the spine head invasion of back-propagating action potential (bAP) and steady-state stimuli (SSS). Voltage invasion (Volt. Inv.) during bAPs and SSS. (*A*) Because we explore the backward propagation of signals into spines, only the resistivity (ρ) value was changed in these simulations. (*B*) Voltage responses in the soma, the dendrite at the position of the relevant spine, and the spine head itself were recorded for somatically evoked bAPs and steady-state current injection (a pulse generated by a 40-ms current injection of 0.3 nA). (*C*) The ratio of the maximally evoked spine head and dendritic response (spine head maximal voltage/dendrite maximal voltage) were defined as the voltage invasion (Volt. Inv.) and recorded for a broad range of ρ for bAPs and SSS [*Upper* and *Lower* of each of the nine (*i–ix*) spine simulations described in Fig. 5]. The dashed vertical line in each panel marks the

Legend continued on following page

value of ρ found on Fig. 5 for which a single conductance (g) value reproduced both experimental findings (neck length and EPSP size) in the forward direction. (*D*) Voltage invasion in long- and short-necked spines at all of the tested ρ values in Fig. 5 for bAPs and SSS (*Upper* and *Lower*, respectively). (*E*) Difference of voltage invasion (ΔVolt. Inv.) in short- and long-necked spines as a function of resistivity value ρ for bAPs and SSS (*Upper* and *Lower*, respectively). (*F*) Translation of electrotonic ρ values into neck resistances (R) for long-necked and short-necked spines plotted against the Volt. Inv. of bAP and SSS.